Q. J. R. Meteorol. Soc. (1987), **113**, pp. 713–734 551.465

Potential vorticity in models of the ocean circulation

By KIRK BRYAN

Geophysical Fluid Dynamics Laboratory/NOAA, Princeton University, Princeton, New Jersey 08540

(Symons Memorial Lecture, 21 May 1986)

SUMMARY

Existing observations suffice to give a qualitative description of the wind-driven and thermohaline components of the ocean circulation, but a hierarchy of analytical and numerical models is now needed for use in coupled ocean–atmosphere models of the earth's climate. Potential vorticity is a more appropriate diagnostic field variable than angular momentum for the ocean circulation because of the complicated geometry of ocean basins. Patterns of potential vorticity on surfaces of constant density help validate ocean circulation models, and give physical insight into how the ocean circulation works.

High resolution models suggest that the lateral mixing of potential vorticity by mesoscale eddies along isopycnal surfaces is of the same order as large-scale advection, and that the assumption of inviscid, potential-vorticity-conserving flow in the thermocline is not appropriate for the real ocean. A satisfactory test of this conjecture will require the extensive measurements planned for the World Ocean Circulation Experiment.

Models also indicate that the transport of water mass properties by mesoscale eddies is largely a mixing along isopycnal surfaces. The weak temperature gradients along isopycnal surfaces in most areas of the ocean limit the effectiveness of the mesoscale eddies in transporting significant amounts of heat across latitude circles.

1. INTRODUCTION

Over 20 years ago an unassuming visitor from Britain brought to my attention some interesting problems related to dynamics of the Antarctic Circumpolar Current. We agreed to meet again the following summer in La Jolla, California, to continue our discussions. This was my introduction to Adrian Gill, and the beginning of a long friendship and scientific collaboration. The foundations for much of the ocean-modelling research discussed in this review were laid during several extended visits by Adrian Gill to Princeton.

In atmospheric science, we take numerical models for granted in developing an understanding of the earth's climate. In oceanography, however, models of the ocean circulation are only beginning to be appreciated as an important research tool. Building numerical models of the ocean circulation has largely been motivated by a perceived need to develop combined ocean–atmosphere models to study climate, rather than a need to understand the ocean circulation, *per se*. A key factor for this difference in approach to modelling in oceanography and meteorology is related to the data bases available in the two sciences. For the atmosphere, global synoptic data are gathered continuously by means of a remarkable communications network. Large-scale numerical models of the atmosphere are an essential tool for interpreting the tremendous flow of data received daily. In oceanography, on the other hand, most data sets tend to be local in both space and time. To obtain deep sea measurements requires a great deal of ship time and skilled human effort. In most cases, global models of ocean circulation would be of little use in interpreting the results of a single oceanographic expedition.

The lack of synoptic data in oceanography has been a more severe handicap than is commonly realized. The initial exploration of the ocean in the first half of the present century produced a simple picture of the distribution of temperature and salinity in the global ocean. The oceanographic equivalent of air masses are water masses defined by the temperature and salinity. Rapid water mass conversion tends to be highly localized in the ocean. While air masses tend to be ephemeral, water masses can be traced for many years and thousands of kilometres from their point of origin (Reid 1965). Although recent hydrographic expeditions have been able to refine the picture of the global water masses, the basic description obtained prior to 1940 has not been substantially changed.

In the absence of a complete synoptic data set for the ocean, additional isolated measurements are of limited usefulness, Fortunately, instruments mounted on satellite platforms promise a partial solution to the lack of synoptic data. Their measurements of surface colour, temperature and topography will provide continuous global data sets. These synoptic data sets can be used, in turn, to provide a context for local sub-surface measurements made from automated platforms, ships of opportunity or research vessels. When satellites have ushered in the era of synoptic oceanography, numerical models will be needed to interpret the expanded oceanographic data base, and modelling will assume the importance it has for the atmosphere.

An illustration of the classical hydrographic data base of oceanography is given in Fig. 1. This meridional section of salinity (Reid 1965) was taken just east of the date line in the Pacific. The upper kilometre has an expanded scale to show the details of the thermocline. Except in polar regions near the surface, the density of sea water is largely controlled by temperature, rather than by salinity. Thus, salinity is an excellent tracer for the deep circulation. The highest surface salinity in Fig. 1 occurs in the subtropical areas of high evaporation and low precipitation. Low salinity waters form in mid-latitude areas of high rainfall. The abrupt, nearly vertical salinity front near 60°S coincides with the very deep penetration of the Antarctic Circumpolar Current. Tongues of low salinity water at the base of the thermocline trace the equatorward movement of the intermediate waters. The conservation of salinity and temperature of slowly moving water masses is a very remarkable characteristic of the ocean, which clearly sets it apart from the atmosphere.

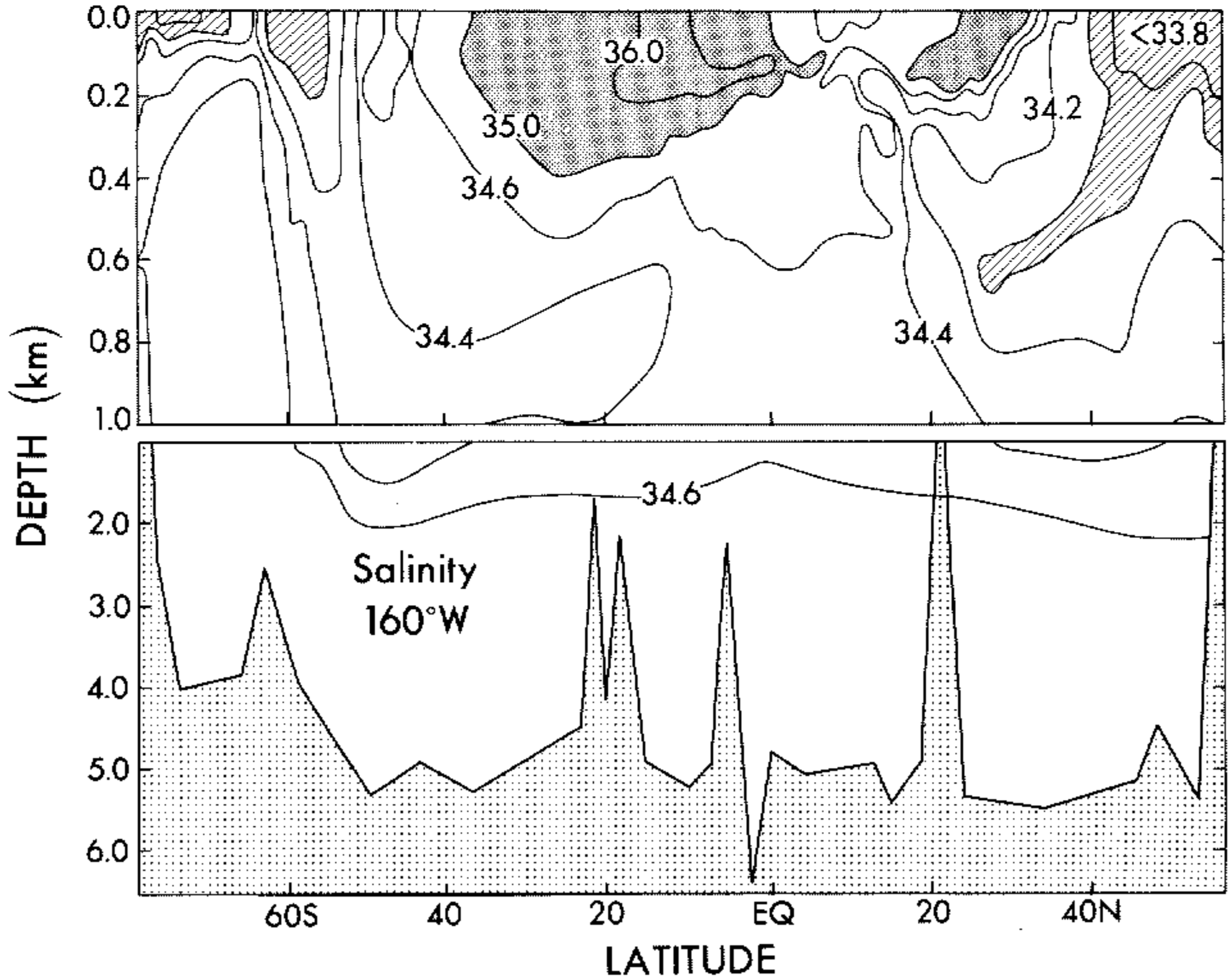

Figure 1. The pattern of salinity (per mil) along approximately 160°W from Antarctica to Alaska (from Reid 1965).

The horizontal view of the depth of a surface of constant density surface in Fig. 2 (Keffer 1985) illustrates the topography of the thermocline in the Pacific. Note that the pattern is dominated by two large depressions, each corresponding to the subtropical wind gyre in its hemisphere. Ekman transport is poleward in the trade wind zone, and equatorward in the area of westerlies. These two great depressions in the thermocline therefore coincide with the regions of wind-forced convergence of surface waters. Looking at the pattern in Fig. 2, one gets the impression of an ocean circulation largely determined by the surface winds, while Fig. 1 suggests a circulation driven by the density gradients caused by the surface sources and sinks of heat and fresh water. This illustrates a dichotomy in the viewpoints of oceanographers with respect to the ocean circulation. Attempts have been made to treat the forcing due to wind and buoyancy sources separately, and then combine the results. However, there is no justification for the assumption of linearity implicit in this approach.

Since small, but significant, secular changes in the water mass properties of the deep ocean have been detected only recently (Roemmich and Wunsch 1985; Brewer *et al.* 1983), classical methods of water mass interpretation tend to be based on the assumption that water masses are stationary with respect to time. Measurements of carbon-14 in the deep ocean have added a 'clock' to water mass analysis, allowing an estimate of the time that has elapsed since the water masses formed at the surface. Tracing the trajectories of water masses, using radioactive tracers and the geostrophic 'thermal wind' relation, have provided an intricate and beautiful picture of the deep ocean circulation, but the description is still qualitative. This is unsatisfactory if we wish to apply our existing knowledge of the ocean circulation to climate and global geochemical cycles and if we wish to develop a capacity to predict the response of the ocean circulation to different external boundary conditions. In particular, there is an urgent need to understand how a coupled ocean–atmosphere system responds to the build-up of the radiatively active, anthropogenic gases.

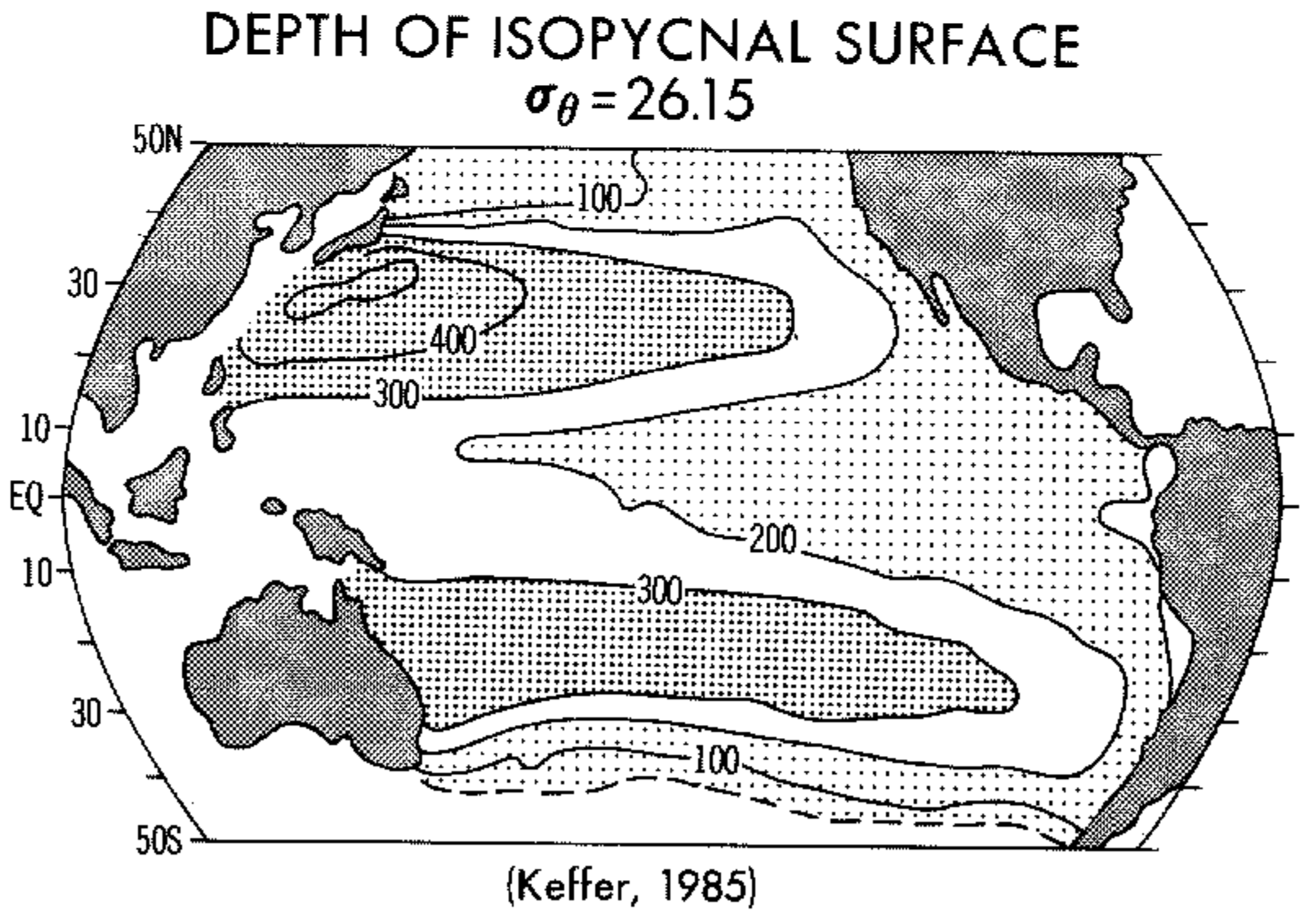

Figure 2. The depth of the $\sigma_\theta = 26{\cdot}15$ surface in the Pacific Ocean in metres (from Keffer 1985). $\sigma_\theta = (\rho^{-1}) \times 10^{-3}$, where ρ is the potential density referenced to the surface.

2. Potential vorticity as a diagnostic field variable

Will it be possible to disentangle the different contributions of wind-forcing and buoyancy flux in driving the ocean circulation with the data we have in hand? The atmosphere has been extensively investigated from the standpoint of the angular momentum budget. An explanation of the atmospheric zonal wind structure is considered tantamount to explaining the general circulation. The circulation of the ocean at most latitudes is confined by continental boundaries. As Rhines (1986) has pointed out, the difficulty of calculating pressure forces at the boundaries makes zonal momentum a less useful diagnostic quantity for ocean dynamics. Vorticity is a more natural diagnostic quantity, and classical theories of the wind-driven ocean by Sverdrup (1947), Stommel (1948) and Munk (1950) are all based on vorticity balance. Potential vorticity was introduced into thermocline theories by Welander (1959) and others. It should be noted that potential vorticity analysis on isopycnal surfaces is receiving renewed attention by meteorologists as well (Hoskins *et al.* 1985).

Rhines (1986) reviews recent progress in applying potential vorticity concepts to the ocean circulation. The present review discusses some of the same observational data and numerical modelling results, but from a somewhat different perspective. This review places less emphasis on dynamics, and is slanted by the author's long term interest in the role of the ocean in climate. The two reviews should be complementary, offering a deeper insight into contemporary problems in understanding and modelling the ocean circulation.

As a diagnostic tool for the large-scale ocean circulation, we can approximate the potential vorticity (*PV* hereafter) by the product of the vorticity about the z axis and the vertical gradient of density:

$$PV = (\zeta + f)N^2/g \tag{1}$$

where ζ is the relative vorticity, f is the Coriolis parameter; N, the Brunt–Väisälä frequency; and g the acceleration of gravity. Note that *PV* is defined in such a way that it is positive for a resting, stably stratified region of the ocean in the northern hemisphere. Away from strong currents, the ratio of $|\zeta|$ to f is much less than unity, and *PV* can be expressed as

$$PV \cong fN^2/g. \tag{2}$$

As pointed out in a recent review by Hoskins *et al.* (1985), potential vorticity has two properties that make it a particularly useful diagnostic tool: (1) *PV*, in a more general form than given in Eq. (1), is conserved along trajectories for adiabatic, frictionless flow, and so in some circumstances, can act as a tracer of water masses; (2) velocity can be derived from a known *PV* field. Hoskins *et al.* call the second property 'invertibility'. When ζ is of the same order as f (Rossby number order of unity), the inversion must be done globally and it involves solving second-order partial differential equations in three dimensions. Away from strong currents Eq. (2) provides a good approximation. In this case, a different type of inversion can be done locally. Hydrographic data, which are measurements of temperature and salinity, provide a basis for computing the geostrophic shear. A classical problem in oceanography is the determination of a reference value to fix the velocities in the water column once the shape of the profile has been determined from the 'thermal wind' relation. Schott and Stommel (1978) first proposed a simple inversion to find the reference velocity. In their method the tracer property of *PV* is used to determine the direction of flow as a function of depth. This information is then combined with the geostrophic shear to find the best fit for a reference velocity. Recently, a very detailed application of this local invertibility principle has been carried out for the

North Atlantic by Olbers *et al.* (1985) using the hydrographic data set of Levitus (1982). Their study explores in detail the information content of the data in this type of analysis and estimates the maximum values of the lateral and vertical mixing as well as the geostrophic reference velocity for the North Atlantic.

3. Theories for the potential vorticity distribution in the thermocline

To introduce recent theories of the thermocline, let us examine Fig. 3, which is the pattern of geostrophic flow on a surface of constant density in the eddy-resolving calculation of Cox (1985). The model is driven by both wind stress and buoyancy fluxes. Figure 3 shows the Montgomery function,

$$M = p + \rho g z \tag{3}$$

on a density surface which outcrops in middle latitudes, p being pressure, and ρ density. The geostrophic streamlines indicate that fluid enters along the outcrop and then moves

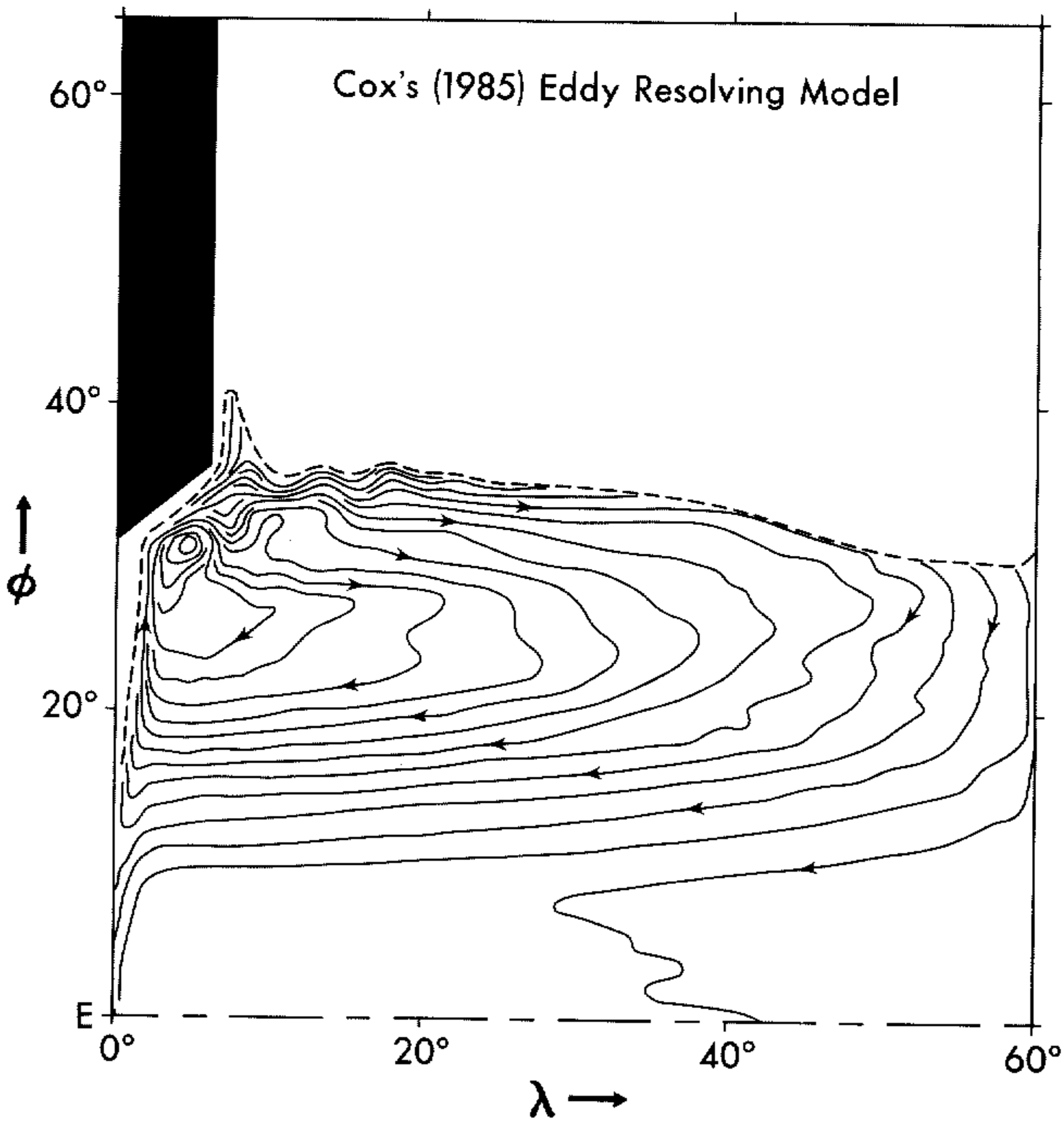

Figure 3. The time-averaged pattern of Montgomery function (geostrophic streamlines) on a surface of constant density in the eddy-resolving model of Cox (1985). Contour interval is 0·05 dyn. metres of equivalent pressure.

downward along the surface of constant density. In other areas streamlines have closed circuits within the isopycnal surface. Rhines and Young (1982; hereafter RY) have called these areas 'pool' regions, and suggested that for an almost 'ideal' (inviscid) fluid flow, *PV* would become uniform along the closed circuits bounding the 'pool' region. If there were no important sources or sinks due to vertical mixing across the isopycnal surfaces, a very small amount of lateral mixing suffices to flush gradients of *PV* within the pool to the outer perimeter. This weak mixing mechanism is advanced by RY to explain the observed fact that *PV* is nearly uniform at the base of the thermocline in the subtropical gyres of the North Atlantic and Pacific.

Luyten *et al.* (1983; hereafter LPS) focus on the region in which geostrophic contours enter the density surface at the outcrop. They term this process 'subduction'. RY emphasize the indirect downward transfer of vorticity by baroclinic instability, while the LPS model, which includes outcrops, emphasizes the direct transfer of *PV* from the surface along downward pathways formed by isopycnal surfaces. LPS suggest that the key to the observed uniformity of *PV* at the base of the thermocline may be that the deeper isopycnals are ventilated by the subarctic gyre waters, which have a rather uniform *PV* at the point of origin. The very different viewpoints embodied in the RY and LPS models will serve as valuable reference points for our review of recent modelling results.

The predictions of the RY theory have been tested in a high resolution, quasi-geostrophic model with eight layers (Holland *et al.* 1984). Results are given in Fig. 4 for the third layer below the surface. Streamlines of flow are shown in Fig. 4(a) and the *PV* pattern for the same level in Fig. 4(b). Holland and Lin (1975) first illustrated how in a purely wind-driven baroclinic model all motion becomes confined to the surface if there is no baroclinic instability or explicit vertical friction to carry momentum downward. Note the existence of a 'pool' region of closed streamlines, and the large region of nearly uniform *PV* in Fig. 4(b). For a resting fluid of uniform stratification, *PV* is a function of latitude only. The forced equatorward flow in the eastern subtropical gyre bows the lines of constant *PV* equatorward. The opposite effect takes place in the subarctic gyre, bowing the lines of *PV* poleward. A large region of nearly constant *PV* is created. Holland *et al.* interpreted the numerical results of the multi-layer, quasi-geostrophic model shown in Fig. 4 to be consistent with the RY theory, although other interpretations were not excluded.

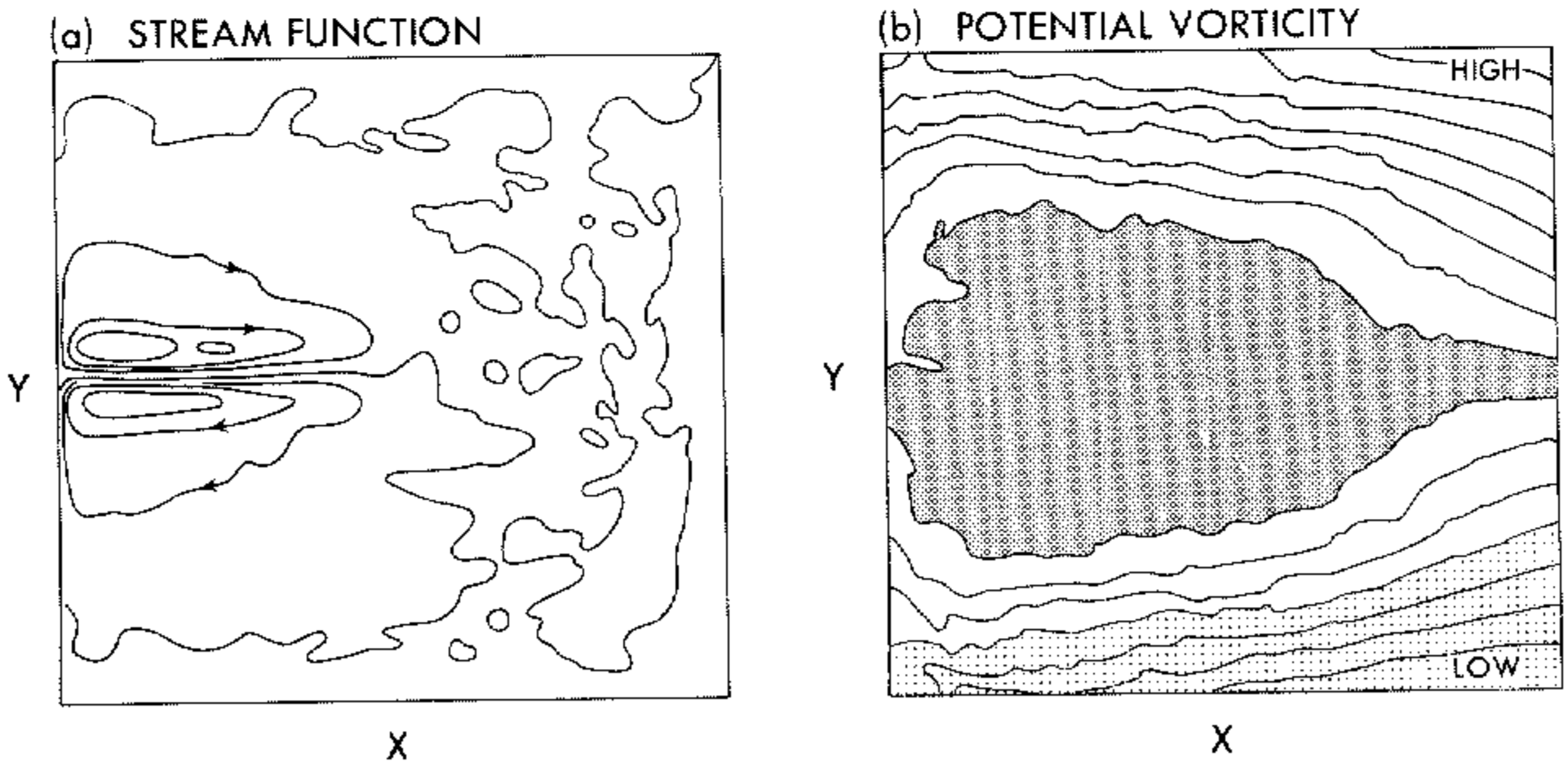

Figure 4. Patterns from an eight-level, eddy-resolving quasi-geostrophic model. (a) Streamfunction on the third level below the surface. (b) Potential vorticity on the third level below the surface. (From Holland *et al.* 1984)

4. Observed potential vorticity fields

The approximate *PV* form given in Eq. (2) is simply the Coriolois parameter multiplied by the local stratification. It can be estimated from the classical hydrographic data set. McDowell *et al.* (1982) have used the North Atlantic IGY data (Fuglister 1960) to map vorticity on isopycnal surfaces. As pointed out above, the observed potential vorticity distributions tend to be rather uniform at the base of the thermocline in the North Atlantic and Pacific. Potential vorticity on a higher isopycnal surface is shown in Fig. 5. At this level, there is obviously structure in the *PV* pattern. Near the eastern boundary and along the southern flank of the subtropical gyre, a ridge of relatively high *PV* coincides with an area of upward displacement of the thermocline. The centre of the gyre is dominated by low *PV* water, which McDowell *et al.* attribute to the equatorward ventilation of water that has undergone winter convection near the outcrop. At the western boundary along the outcrop line, another *PV* maximum occurs in association with the packing of isopycnal surfaces in the Gulf Stream front. As one might expect, there is low *PV* at the equator where the Coriolis parameter goes to zero.

If we compare the *PV* pattern observed in Fig. 5, and the pattern produced by a quasi-geostrophic model, Fig. 4, there are some interesting differences. The pattern in Holland *et al.* (1984) indicates uniform *PV* in the pool region of the subtropical gyre. The *PV* level in the gyre is midway between that found at the northern and southern boundaries. The observations in Fig. 5 show that the pool region is actually occupied by low *PV* waters. Without the winter convection, it would be difficult for any quasi-geostrophic model to simulate this observed subduction of low *PV* waters. The North Pacific data, Fig. 6, show the pattern of *PV* for approximately the same isopycnal surface

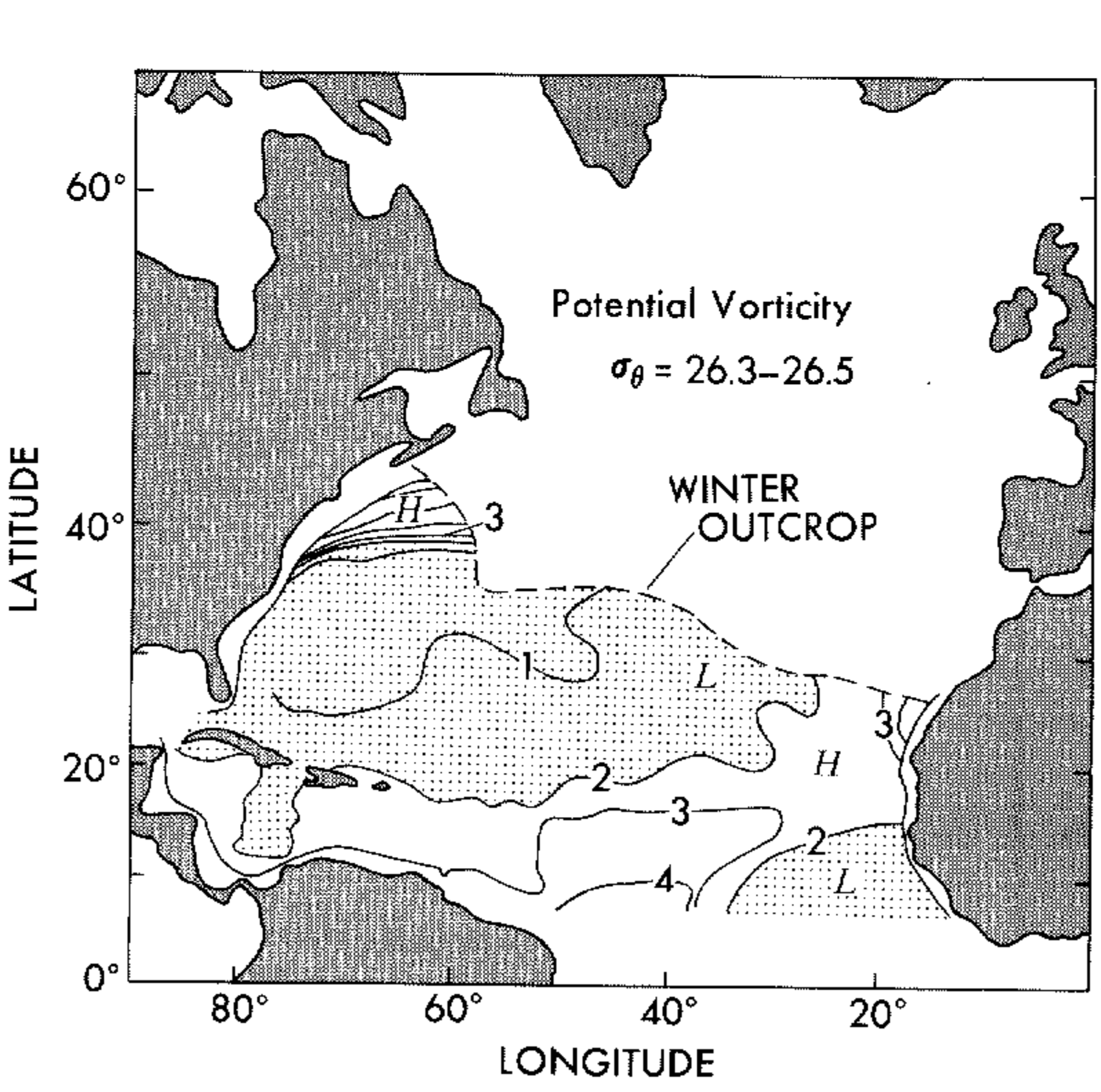

Figure 5. Pattern of potential vorticity based on IGY hydrographic data between the σ_θ surfaces 26·3 and 26·5 (from McDowell *et al.* 1982). Units are 10^{-13}cm^{-1}s^{-1}.

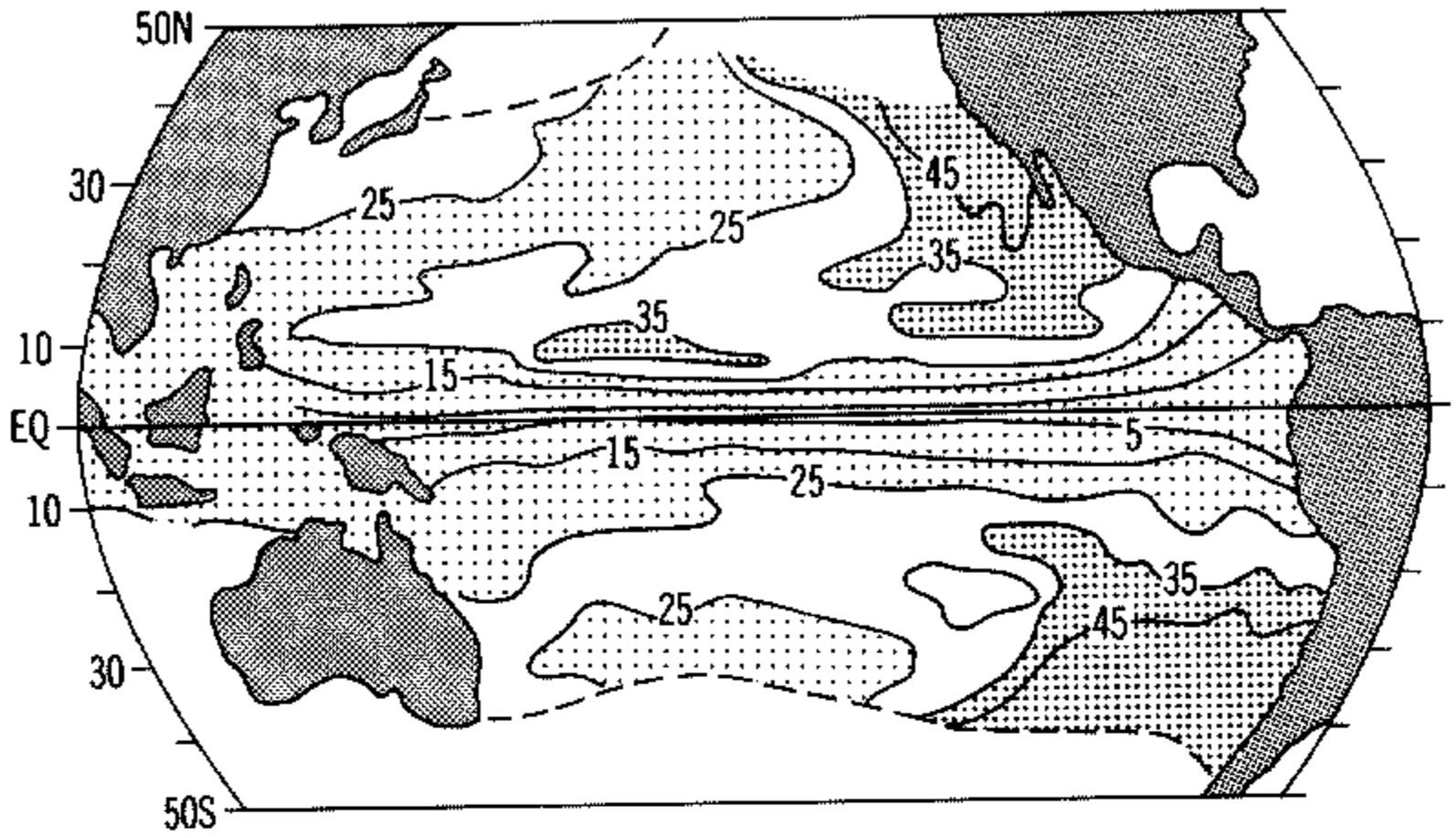

Figure 6. Pattern of potential vorticity in the density interval $\sigma_\theta = 26{\cdot}25$–$26{\cdot}75$ based on the Levitus (1982) data set (from Keffer 1985). Units as in Fig. 5.

as used in Fig. 5. Because the North Pacific waters are less saline and lighter than those of the North Atlantic, however, the same isopycnal surface occupies a lower position in the thermocline and covers a much more extensive area. The depth of this surface is shown in Fig. 2.

In the North Pacific, we see that low *PV* waters occupy a large part of the central basin just as they do in the North Atlantic. There is also the same tendency for *PV* to increase near the western boundary. The two oceans differ in that the Pacific has a very wide region of relatively high *PV* near the eastern boundary while the Atlantic has only a very small area of high *PV* in the corresponding location. This difference may be due to the very great difference in size of the two basins. The area covered by low *PV* water associated with wintertime convection at the outcrop in the Pacific equals or exceeds that in the North Atlantic. However, the size of the Pacific is so much greater it can accommodate a large area with a marine climate. This area is far downwind of the Eurasian continent with little wintertime convection in the upper ocean. Keffer (1985) suggests that the high *PV* waters of the eastern Pacific are associated with the ventilation of low salinity waters in the Gulf of Alaska. The same marine climate prevails in the south-east Pacific, where a similar low salinity tongue forms off the coast of Chile. The tongues of high vorticity water in the North and South Pacific extending in an anticyclonic sense strongly suggest that *PV* is behaving as a tracer in the eastern Pacific, but one must reserve judgement until more detailed observations become available.

5. Numerical experiments based on the primitive equations and isopycnal coordinates

The tendency for water mass properties to be conserved along trajectories of basin-scale, as shown in Fig. 1, indicates that mixing must be extremely small or must take place largely along density surfaces. In conventional numerical models the lateral mixing is along horizontal coordinate surfaces and this tends to give rise to a spurious diabatic mixing in areas of strong horizontal density gradients (Veronis 1975; McDougall and Church 1986). The semi-Lagrangian, isopycnal coordinate system avoids this problem

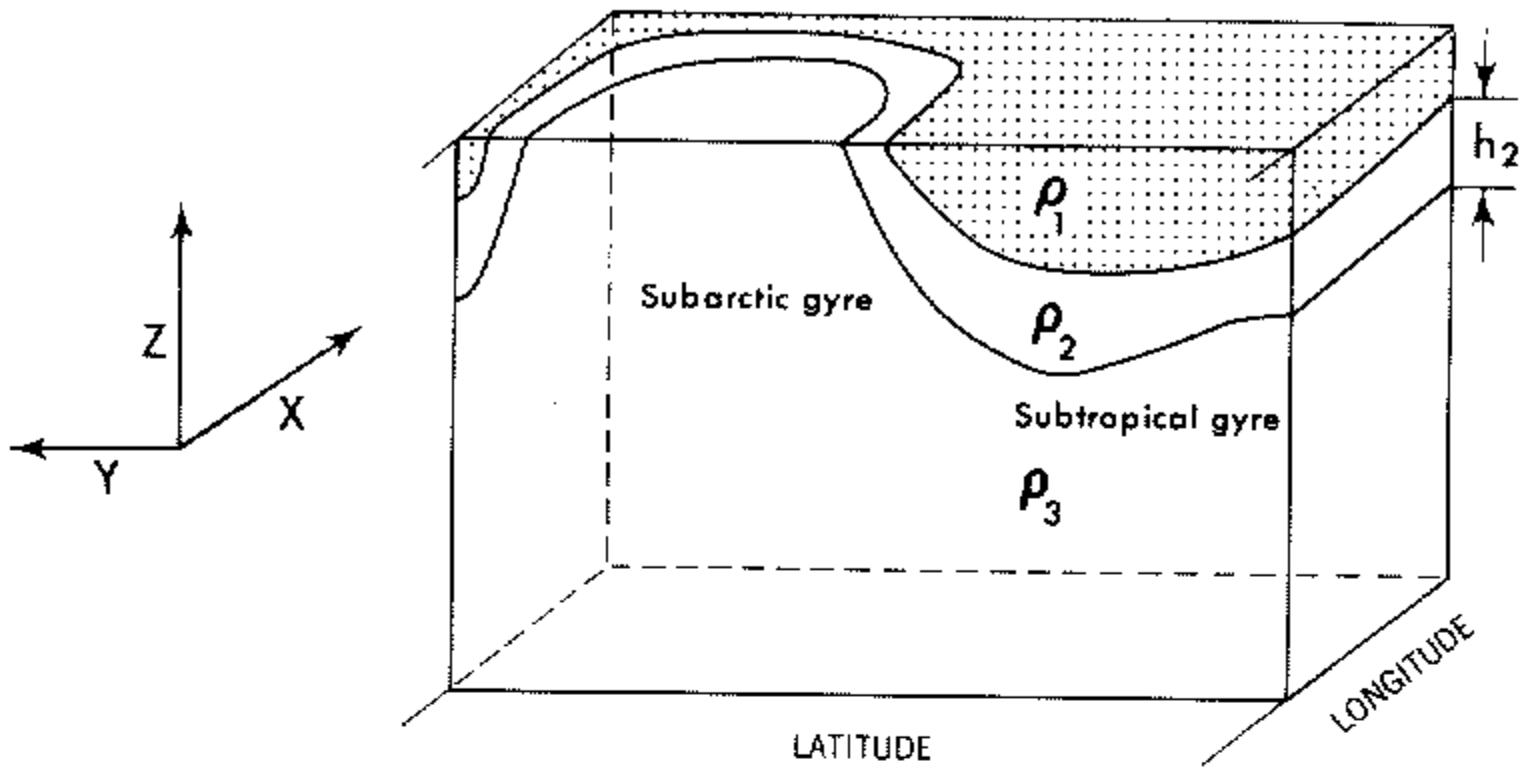

Figure 7. Structure of the three-layered wind-driven model of Huang (1987) based on the primitive equations. The model has two active layers over a deep inactive layer.

because lateral mixing along coordinate surfaces cannot lead to cross-isopycnal fluxes. Pioneering work on isopycnal models has been carried out by Bleck and Boudra (1981) and Schopf and Cane (1983). The additional physical insight that can be gained when an isopycnal coordinate system is used is also very important. This point has been emphasized by Hoskins *et al.* (1985).

A recent study by Huang (1987) serves to illustrate the use of a layered model. The structure of the model is shown in Fig. 7. Two active layers at the surface overlie a deep layer at rest. Ekman pumping in the subtropical gyre forces a surface convergence and downward motion. The opposite process takes place in the subarctic gyre region, where the active layers are pulled up to the surface, causing outcropping. The great advantage of the primitive equation model, compared with quasi-geostrophic models, is that it can

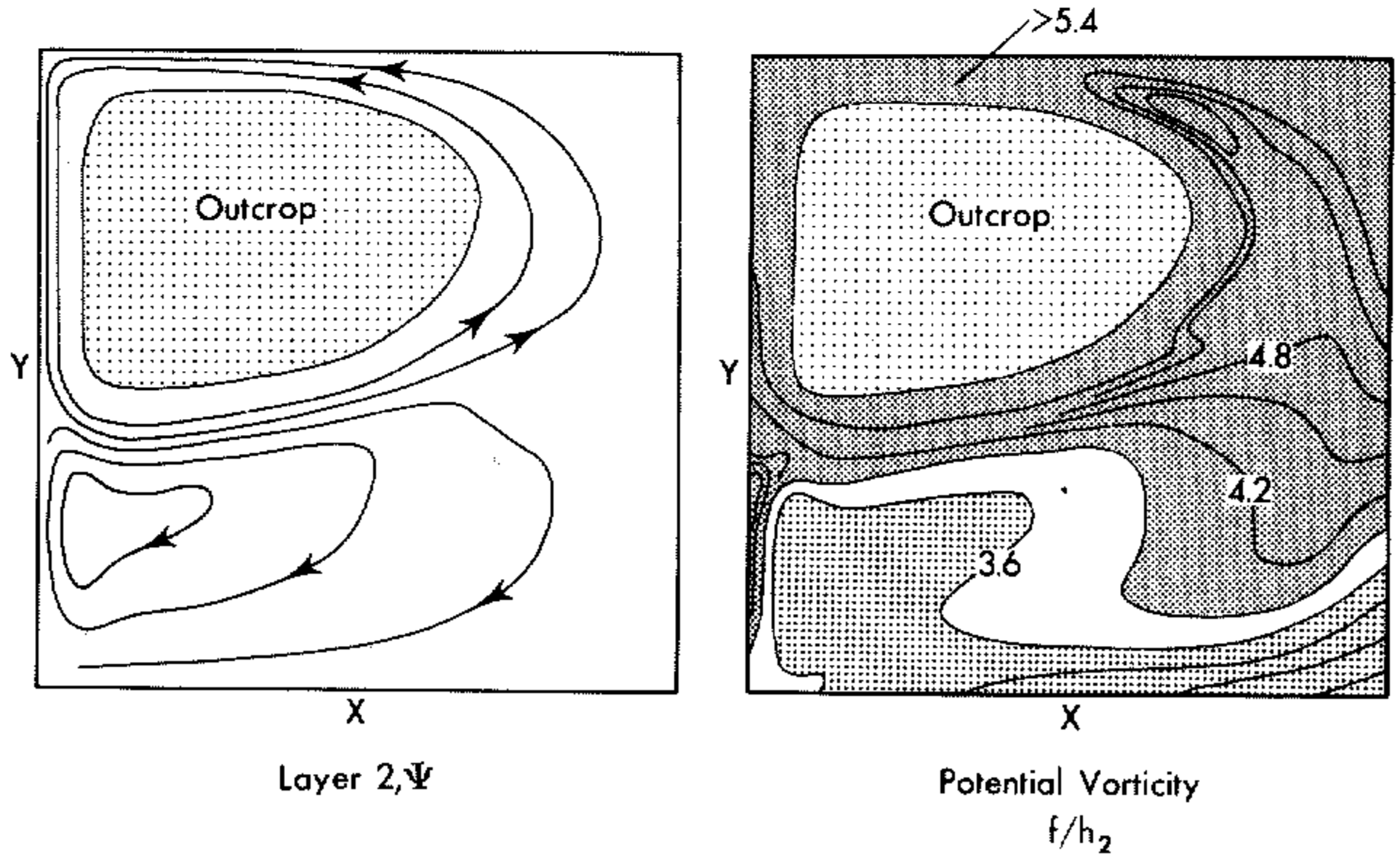

Figure 8. Streamfunction (left panel) and potential vorticity (f/h) (right panel) in the second active layer in Huang's (1987) model.

accommodate outcropping and large changes in layer thickness. The pattern of potential vorticity in the lower active layer is shown in Fig. 8. Unlike the quasi-geostrophic case shown in Fig. 4, the model has insufficient horizontal resolution to resolve mesoscale eddies explicitly, but interfacial friction provides a crude parametrization of the downward momentum transfer of mesoscale eddies. If we compare Fig. 4 and Fig. 8, we see the same tendency for relatively high potential vorticity waters to be advected southward on the eastern side subtropical gyre. On the other hand, the Huang model has another centre of high potential vorticity in the western boundary current, that extends outward along the line separating the gyres. The primitive equation, layered model completely lacks the large area of low potential vorticity water seen in the centre of the Atlantic and Pacific subtropical gyres in Figs. 5 and 6. This is to be expected, since the model is purely wind-driven and lacks the convective overturning needed to produce low potential vorticity water at the outcrop. In the quasi-geostrophic model of Holland *et al.* (1984) a strong gradient of potential vorticity between the subarctic and subtropical wind gyres is present in the surface layer, but not in the deeper layer shown in Fig. 4.

6. An eddy-resolving, primitive equation model

Mesoscale eddies in the ocean are the dynamic counterpart of cyclones and anti-cyclones in the atmosphere, although nearly an order of magnitude smaller in scale. Thus, a greater range of spatial scales must be considered in the ocean than in the atmosphere to obtain the same level of dynamic detail. Oceanographers are only now beginning to use models that are really equivalent to the atmospheric models used routinely in research and forecasting. In the past, difficulties in resolving mesoscale eddies in primitive equation models have led to a heavy reliance on quasi-geostrophic models despite their inability to represent the thermohaline component of the ocean circulation.

As a departure from previous eddy-resolving, quasi-geostrophic models, Cox's (1985) ambitious calculation with an eddy-resolving, primitive equation model is a particularly significant contribution to the goal of more accurate ocean circulation simulations. The pattern of time-averaged flow on a constant density surface in Cox's model has already been shown in Fig. 3. The model simulates flow in a large basin enclosed between two meridians 60° of longitude apart and extending from the equator to 65° of latitude. Since it includes both outcropping and ventilation as well as 'pool' regions, it has the essential physical elements of both the RY and the LPS theories. The numerical experiment was carried out in two stages. In the first stage, an equilibrium, steady-state solution was obtained for the model with 110 km × 110 km resolution and 18 vertical levels. This level of resolution does not allow the existence of mesoscale eddies. They appear in the solution only in the second stage in which the resolution is increased to 37 km × 37 km. Numerical integration in the second stage is carried out for a period of 24 years. While 24 years is not long enough to allow complete adjustment of the deep ocean, Cox shows that it is sufficient for good adjustment of the velocity fields of the upper thermocline.

Patterns of tracer and *PV* along a surface of constant density are shown in Fig. 9. The patterns corresponding to the low resolution, first stage of the numerical experiment are in the two panels on the left. The idealized tracer is specified with a nearly uniform value at the surface and decays with a 20-year half life as it penetrates downward into the interior. The tracer age is estimated from the decay and, in the absence of mixing, measures the time elapsed since a parcel of interior water has visited the surface. Mixing

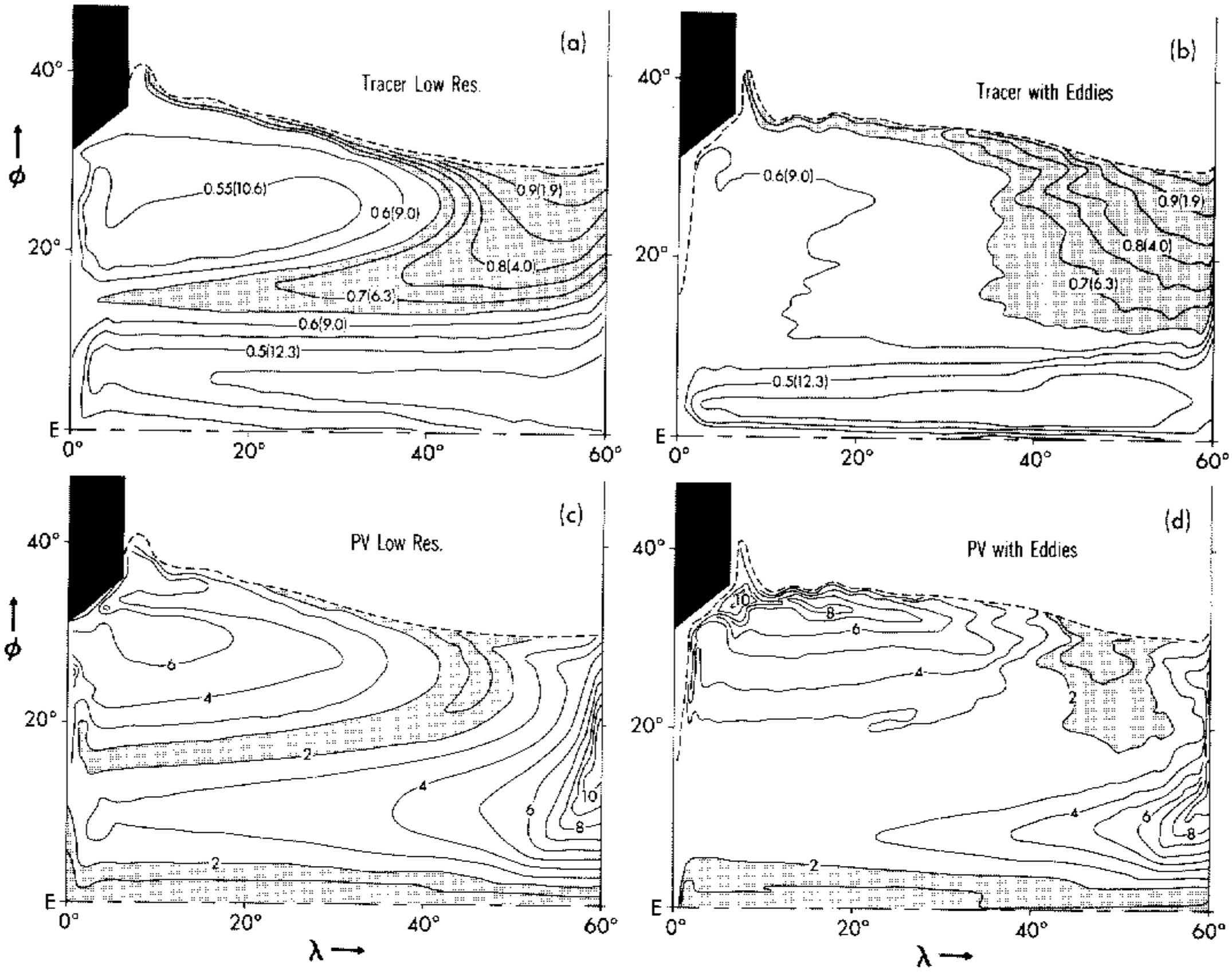

Figure 9. Patterns on density surface from Cox's (1985) 18-level model which includes both wind and buoyancy driving. (a) Tracer patterns for stage one (low resolution without eddies). (b) Tracer pattern with eddies in stage two. (c) *PV* pattern without eddies. (d) *PV* pattern with eddies. Units as in Fig. 5.

biases the tracer age estimated this way, toward lower values. For the first low resolution stage of the experiment, the tracer source at the outcrop is drawn out in a long narrow tongue as it moves equatorward and westward along the isopycnal surface into the interior of the subtropical gyre. The corresponding tracer pattern for stage two, when eddies are present, is shown in Fig. 9(b). Note that the eddies smear the tracer along the density surface, creating a large area of nearly uniform tracer age in the centre of the gyre. Although the explicit, horizontal mixing along level surfaces is much less in stage two, the mixing by mesoscale eddies along the isopycnal surface more than compensates.

The patterns for *PV* shown in Figs. 9(c) and (d) illustrate the same strong mixing by mesoscale eddies along isopycnal surfaces. Low *PV* waters that have undergone convection are subducted into the thermocline from the outcrop line. The low *PV* waters are carried along the eastern and equatorward flank of the gyre on almost the same path as the tracer. The narrow tongue formed in stage one is blurred by mesoscale eddy mixing in stage two. Note the broad interior region where *PV* is nearly uniform and the maxima of *PV* at both the eastern and western boundaries.

As we compare observed patterns of *PV* in the Atlantic and Pacific Oceans, we can identify similar features. The interior of the mode is dominated by low *PV* waters as observed, and high *PV* waters are found at both the eastern and western boundaries. Cox was able to simulate the low *PV* ventilated waters because the model contained a

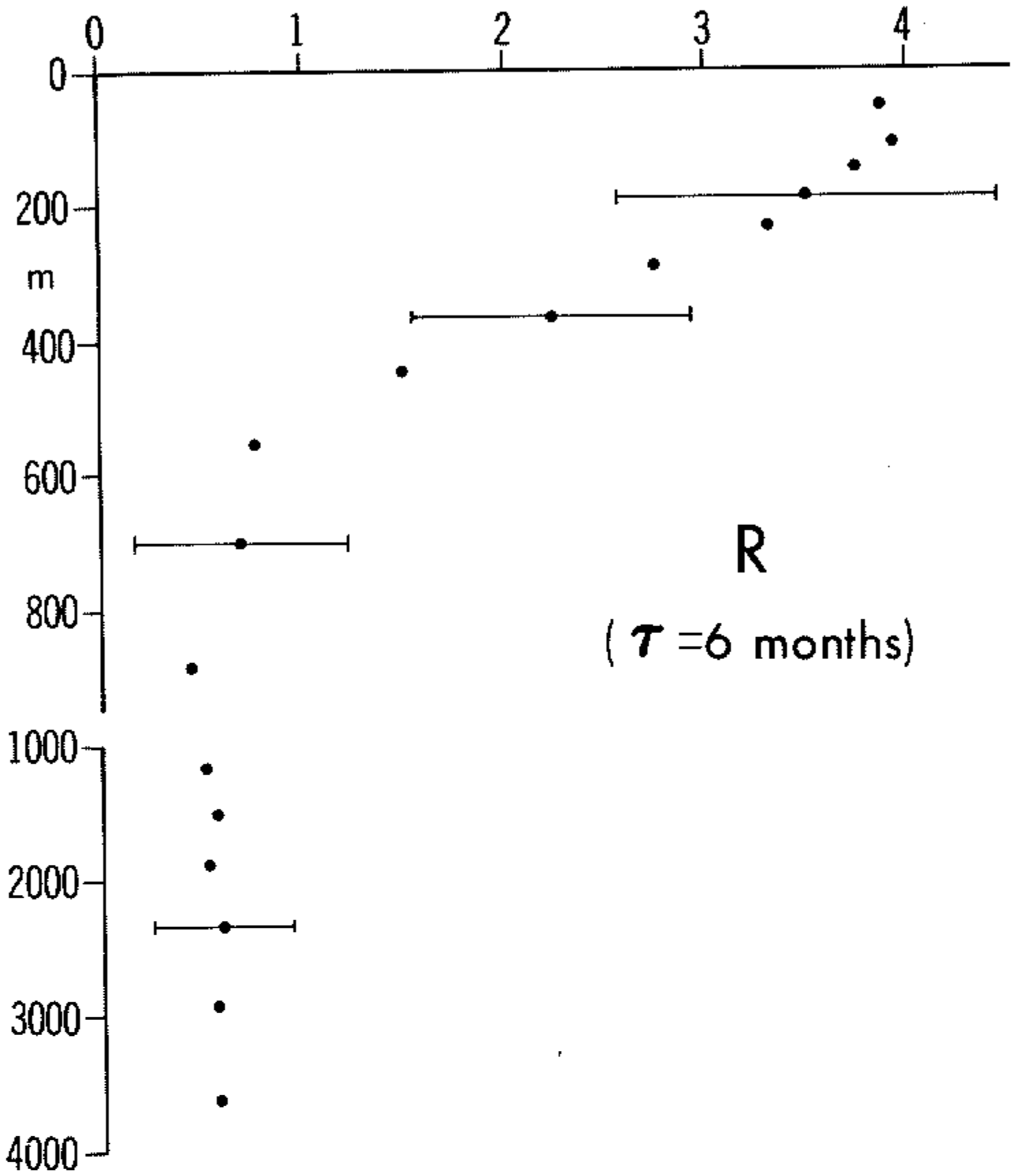

Figure 10. R defined by Eq. (4) as a function of depth in the subtropical gyre from Cox's (1985) model reproduced from Böning and Cox (1988). R provides a measure of the ratio of advection to mixing by mesoscale eddies. The horizontal bars represent the standard error based on ten realizations.

thermohaline circulation, while the purely wind-driven circulation models do not. Figure 9 gives the impression of a circulation that differs from the 'ideal' or 'almost ideal' envisioned in the LPS and RY models, in which the PV is completely or nearly conserved along trajectories. In the Cox model, PV appears to be diffused rapidly along isopycnal surfaces as the subducted water moves away from the outcrop.

The effective diffusivity of Cox's model has recently been calculated by Böning and Cox (1988) using Lagrangian statistics. The results must be considered preliminary, since the model does not fully resolve the full range of mesoscale eddy scales. However, results for the eastern portion of the subtropical gyre indicate levels of 10^3–$10^4 \mathrm{m^2\,s^{-1}}$, in rough agreement with the small amount of data available. A measure of the ratio of advection to diffusion is given by R, where

$$R(t) = |\mathbf{U}|t/(D_x^{1/2} D_y^{1/2})^{1/2} \tag{4}$$

U being the mean particle velocity over a time interval t. The numerator therefore represents the displacement. D_x and D_y are the two orthogonal components of the root mean square displacement. $R(t)$ grows in time as the numerator increases and the denominator asymptotes to a nearly constant value. $R(t)$ is time-dependent, but is a less ambiguous measure of the ratio of advection to mixing than a Péclèt number, for which an arbitrary length scale must be assigned.

Figure 10 reproduces a figure from Böning and Cox. $R(t)$ is shown at six months in

the eastern subtropical gyre. The significant point is that mesoscale eddy mixing penetrates more deeply than the time-averaged velocity in the thermocline. At the base of the thermocline it is obvious that diffusion will dominate over advection. RY and LPS suggest two mechanisms for explaining the homogenization of *PV* at the base of the thermocline. Figure 10 indicates a third mechanism, namely that a strong diffusion will automatically flatten the *PV* distribution at the base of the thermocline where mesoscale eddies dominate. For this 'strong mixing' case the effect of closed streamlines in pool regions is not needed. Contrasts in *PV* of the subducted waters generate baroclinic instability which in turn wipes out the contrasts.

7. Budget of potential vorticity

To gain further insight into the patterns of *PV* on isopycnal surfaces, other diagnostic calculations are helpful. Cox and Bryan (1984) show the change in *PV* along a steady-state trajectory for a low resolution version of the model used by Cox (1985). The results are shown in Fig. 11 for a trajectory that starts in the middle of the subtropical gyre, enters the western boundary current and is finally expelled. It then penetrates the convective zone along the boundary between the subtropical and subarctic gyres. The change in the *PV* along the trajectory is shown, together with the various terms which contribute to the change in the vertical density gradient.

At the beginning of the trajectory, the parcel was well below the surface and the flow was nearly ideal with little change occurring in *PV*. At the western boundary, it turns northward and potential vorticity increases because of an increase in f. Stratification remains nearly constant due to a near balance between advection and lateral diffusion. As the trajectory leaves the western boundary, it enters a strongly convective zone. Convection produces a sharp *PV* loss. The *PV* gradually increases again as the fluid is injected back into the thermocline. Vertical diffusion acting to restore the stratification over-compensates for the fact that the particle is moving southward into a region of lower Coriolis force.

Figure 11 illustrates only one special trajectory. To get a better overall view, we can average over many trajectories in the meridional plane. Let θ be the temperature, which is directly proportional to buoyancy in the Cox (1985) model, and ϕ and λ be the latitude and longitude. Let a be the radius of the earth and $\lambda 2$ the longitude of the eastern wall of the basin. It is possible to define a mass-transport streamfunction in the θ–ϕ (temperature–latitude) plane:

$$\partial_\theta \psi = -\int_0^{\lambda 2} \rho V(\partial z/\partial \theta) a \cos\phi \, d\lambda \tag{5}$$

$$\frac{1}{a}\partial_\phi \psi = \int_0^{\lambda 2} \rho \dot{\theta}(\partial z/\partial \theta) a \cos\phi \, d\lambda. \tag{6}$$

The gradient, $\partial_\theta \psi$, provides a measure of the total meridional transport integrated zonally across the entire basin along temperature surfaces. The field, $\dot{\theta}$, represents the flow of water across isopycnal surfaces, forced by the vertical and horizontal mixing and the convective overturning. It is this cross-isopycnal flow that drives the thermohaline component of the circulation.

There are several regions in which the cross-isopycnal flow dominates. These regions can be seen in Fig. 12(a) for the zonally averaged transport of heat in Cox's eddy-resolving model. The most important location is near the surface boundary where the

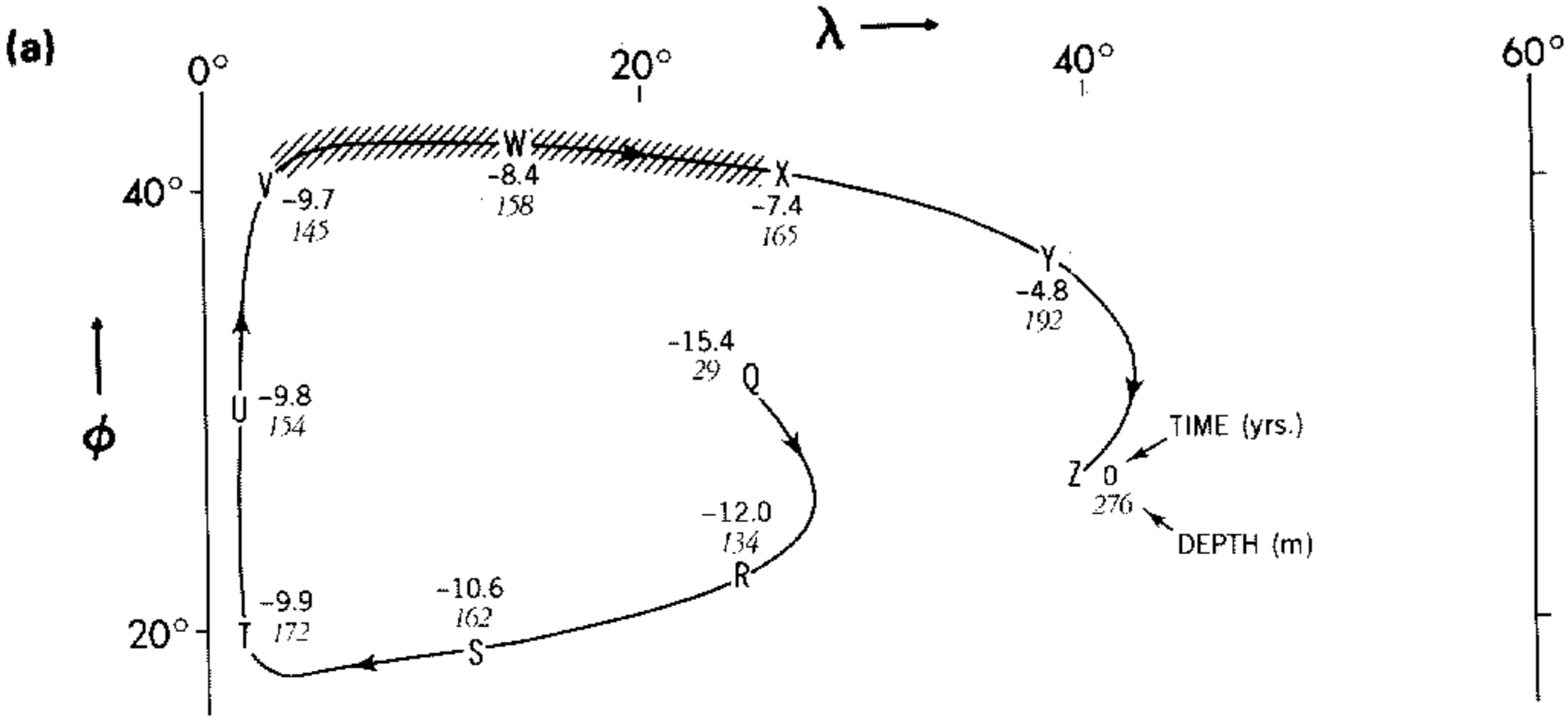

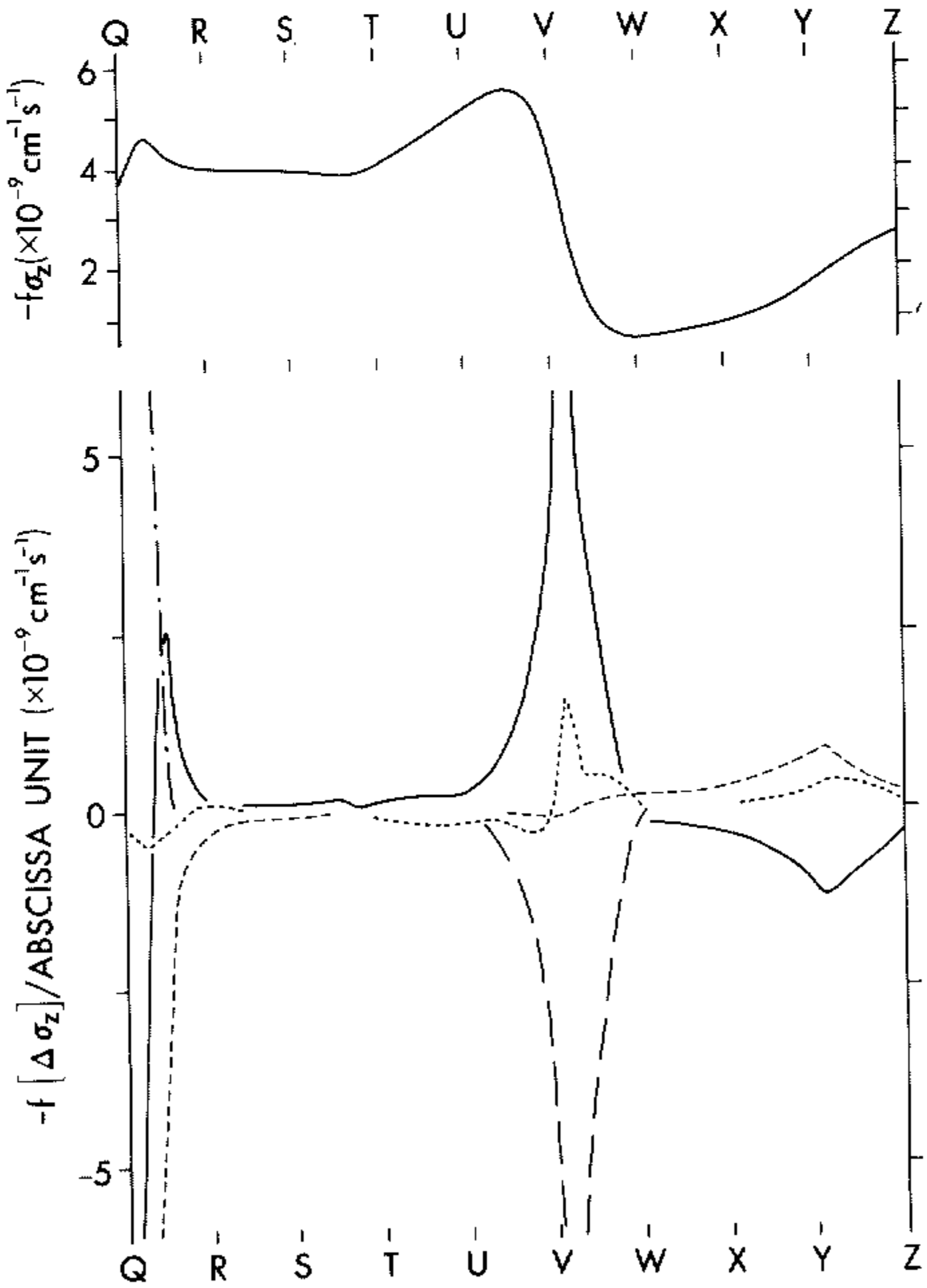

Figure 11. (a) A particle trajectory in the steady-state solution of Cox and Bryan (1984). (b) The change in *PV* along the trajectory. (c) The important terms changing the stratification with respect to time along the trajectory. Long dashes—convection. Solid—advection. Dots—horizontal mixing. Short dashes—vertical mixing.

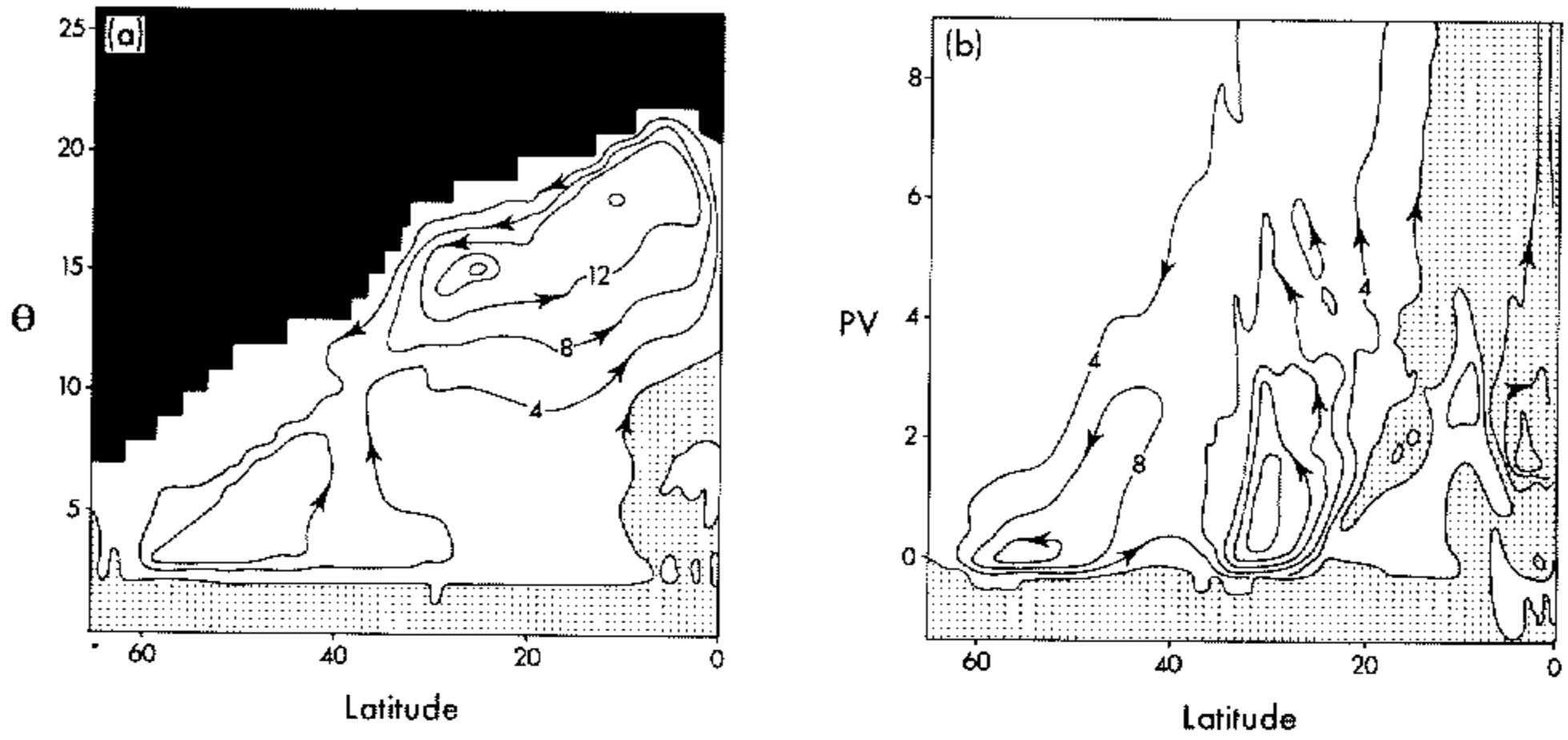

Figure 12. Diagnostic analysis from the eddy-resolving model of Cox (1985). (a) The zonally integrated mass transport streamfunction in the temperature–latitudinal plane. (b) The mass transport in the *PV*–latitudinal plane. The ordinate in (b) has the same units for *PV* as in Fig. 5. The mass transport is in units of megatons per second.

forcing by the external boundary conditions allows a strong cross-isopycnal flow. The dominant feature is the strong cooling produced when water at the surface moves from low to high latitudes. Cross-isopycnal flow is also very important at the equator, where the thermocline is pinched upward and intense upwelling at the equator must be balanced by downward mixing. Note that the poleward flow at the surface is interrupted in mid-latitudes, and a branch is injected back into the thermocline. This feature corresponds to the ventilation process envisioned for the LPS model: the wind drives surface waters downward along the isopycnal surfaces, injecting them into the thermocline. The injected flow tends to move equatorward along isopycnal surfaces. At the poleward wall, the stratification vanishes and the entire water column has almost uniform low temperature. As the deep water flows equatorward along the bottom, vertical mixing slowly incorporates it into the thermocline. The strong transport across isopycnals does not necessarily imply that mixing is more rapid at the base of the thermocline than elsewhere, only the relative weakness of competing processes.

A similar transport diagram in which *PV* is the ordinate is shown in Fig. 12(b). In this diagram, the *PV* definition includes the relative vorticity, but it is still approximately a measure of the vertical derivative of temperature multiplied by the Coriolis term. Figure 12(b) gives a quantitative picture of the total exchange of *PV* between low and high latitudes. The diagram is dominated by two counterclockwise cells, one in middle latitudes, and one in polar latitudes. Both cells transport high *PV* waters poleward from the source regions in low and middle latitudes to the sink regions in high latitudes. The sources of high *PV* include all the thermodynamic and dynamic effects that cause the water to become more stratified. Convection dominates the *PV* loss. The two cells correspond to the two counterclockwise cells in Fig. 12(a).

The counterclockwise cell in middle latitudes may be identified with the transport of high *PV* waters in the western boundary current, and with the subsequent loss of *PV* in the convective zone in the outflow region between the subtropical and subarctic gyres. The sequence resembles that shown for the low resolution case shown in Fig. 11. In the present case, the destratified waters are reinjected back into the thermocline by the wind-driven subduction. The smaller cell in polar latitudes is associated with the formation of

the abyssal waters near the northern wall. A clockwise cell, transporting PV equatorward, forms near the equator. Well-stratified thermocline water converges on the equator, and poorly-stratified, Ekman drift diverges from the equator.

8. Mesoscale eddies and poleward heat transport

How important are the mesoscale eddies in the heat balance of the World Ocean? In the atmosphere, synoptic-scale motions in mid-latitudes play a dominant role in poleward heat transport. Mesoscale eddies in the ocean are the dynamic equivalent to synoptic-scale disturbances in the atmosphere. *A priori* reasoning would suggest that mesoscale eddies would be important in poleward heat transport in those regions where they are very energetic. However, model results (Bryan 1986) suggest that the situation is much more complicated. Some important questions are raised by the models that can only be settled by future field measurements.

The two model studies that are particularly useful for examining the poleward eddy heat transport are those of Semtner and Mintz (1977) and the much more complete calculation by Cox (1985) mentioned earlier. Both include the mesoscale eddies in a model with the thermohaline circulation. Neither study is ideal for examining heat transport questions because separate heat and salinity fields are not included explicitly. The solutions only allow statements about the contribution of the mesoscale eddies to the buoyancy transport. The results apply to the real ocean in regions where heat and buoyancy are well correlated, keeping in mind that there are many situations in which heat and buoyancy are *not* well correlated, e.g. the polar haloclines and the warm core rings.

In both models the buoyancy flux through the ocean surface is proportional to the difference between the buoyancy in the mixed layer and a prescribed reference buoyancy at the surface which decreases linearly with latitude. In the final solution presented in Cox's paper, the *in situ* poleward buoyancy transport divergence agrees with the surface flux, and thus indicates a reasonable equilibrium adjustment of the density field. The buoyancy transports for the high- and low-resolution cases are compared in Fig. 13. The ordinate is labelled heat transport only because the heat and buoyancy transport are equivalent in this simple model. The low resolution model does not allow mesoscale eddies. Transport by the time-varying motions in the high resolution case is mainly toward the equator. A more detailed analysis (not shown) indicates that this equatorward flux in the subtropical gyre is due to the baroclinic instability of the westward flow, as envisioned by Gill *et al.* (1974). Since the thermocline tilts upward toward the equator, the down-gradient flux is towards the equator rather than towards the pole.

Note that the augmentation of the transport by the time-averaged flow in the high resolution case increases the poleward transport in the same latitude range. It is interesting that the total poleward buoyancy flux is nearly the same in both the eddy-resolving and the non-eddy-resolving cases! It turns out that the augmentation to the poleward buoyancy (or heat) transport by the time-averaged motions is also wave-induced. This transport is caused by a meridional cell shown in Fig. 14. The cell has an upper poleward-moving branch and a lower equatorward return flow in the main thermocline. Because the thermocline slopes upward toward the equator, the circulation induced by the eddies is thermally indirect. In this sense it is like the Ferrel cell in the atmosphere, as suggested by Mintz (1979). Unlike the Ferrel cell, however, the overturning can be geostrophically balanced by a net pressure difference between the meridional walls at the boundaries. This discussion has focused on the Cox model rather than the Semtner and Mintz model

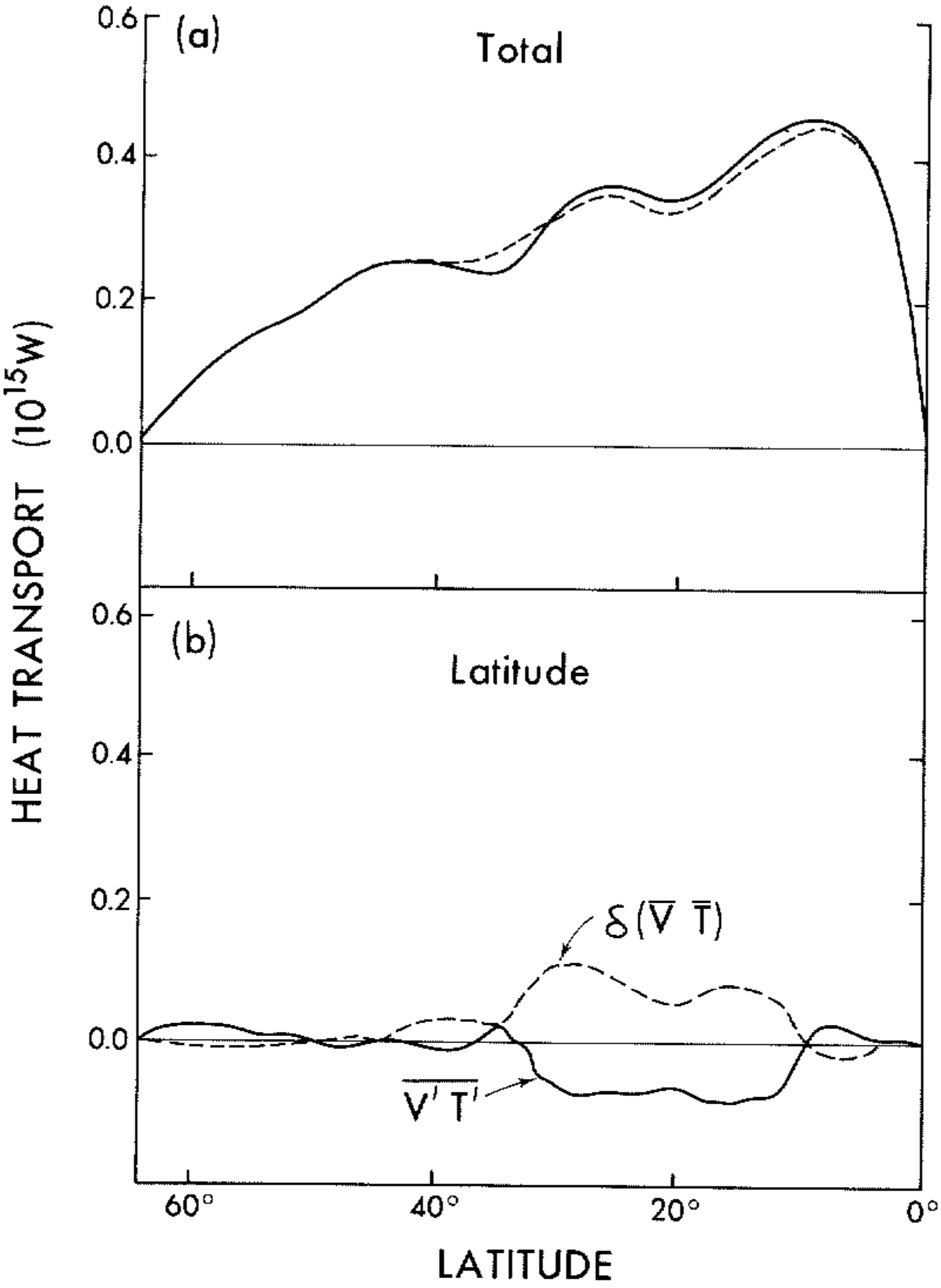

Figure 13. (a) Total time-averaged buoyancy from Cox's (1985) model: the eddy-resolving model (solid) and the coarse resolution, non-eddy-resolving model (dashed). (b) Heat flux due to transient fluctuations (solid) and the enhanced transport by time-averaged motions in the eddy-resolving model. (From Bryan 1986)

because it has not been possible to analyse the latter in detail. The published results appear consistent.

What is the physics behind these apparently complex, buoyancy transport signatures? In the model, the density tends to be conserved along the trajectories associated with the mesoscale waves. Consider the case of small amplitude in a system with a horizontally uniform buoyancy gradient in the y and z directions. The perturbation buoyancy can be expressed in terms of displacements, Y' and Z', as

$$B' = -Z'\partial_z B_0 - Y'\partial_y B_0. \tag{7}$$

On multiplying Eq. (7) by v' and averaging with respect to time, the buoyancy transport is

$$\overline{v'B'} = -\overline{v'Z'}\,\partial_z B_0 \tag{8}$$

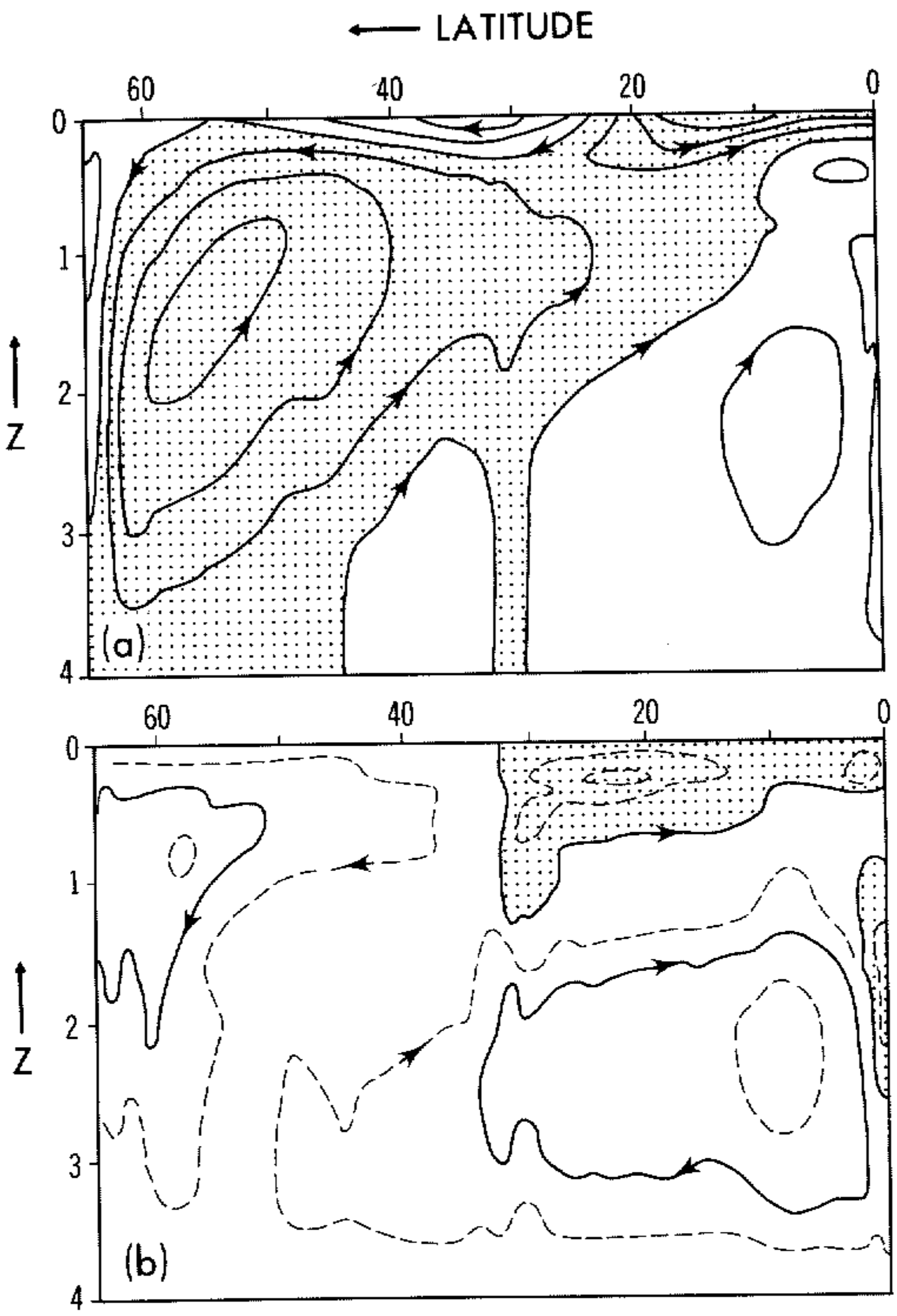

Figure 14. (a) The total time-averaged mass transport in the meridional–depth plane in Cox's (1985) model. (b) The enhanced circulation due to high resolution and existence of eddies. Note the shallow counterclockwise cell in the subtropical gyre. (From Bryan 1986)

since v' and Y' are in quadrature. Imagine a train of baroclinic eddies in the westward flow on the equatorward flank of the subtropical gyre. The trajectory of a buoyancy-conserving particle would be a spiral about the x axis. Looking downstream (westward) the loops would be clockwise, and would transport the light, buoyant surface waters poleward, and the heavier, deeper water equatorward. In the ideal density-conserving case this transport by a vertical cell is exactly compensated by the $v'B'$ correlation.

This idealized model shows the conceptual difficulty of designating transport due to time-varying motions as 'eddy' transport. Such terminology neglects the wave-induced, time-averaged flows that are also associated with the mesoscale eddies. If field measurements of the transport of heat and tracers by the mesoscale eddies are attempted, they should be designed to measure both components of eddy transport: that part due

to time-varying motion and that part due to wave-induced, time-averaged flows. The need to measure two components of transport is artificial, caused by viewing transport in an Eulerian framework. Lagrangian instruments that move along an isopycnal surface would measure transport by mesoscale eddies much more easily. Drifters of this type are now under development at Woods Hole.

If it is recognized that the mixing produced by the mesoscale eddies is a tensor that is primarily aligned with the isopycnal surfaces, then it is clear that in a steady state only quantities that have gradients along isopycnal surfaces will be mixed. As pointed out above, buoyancy is uniform along an isopycnal surface and is not mixed by trajectories within isopycnal surfaces. On the other hand, the strong *PV* gradients in the upper thermocline shown in Figs. 5 and 6 allow the *PV* mixing by mesoscale eddies illustrated in Fig. 9. The transient tracers can also be strongly mixed, because they also have strong gradients along the isopycnals when they are first injected into the thermocline. Observations show that temperatures in middle latitudes are highly correlated with density and, therefore, have rather weak gradients along the isopycnal surfaces. Thus, in a steady state mesoscale eddies will not mix heat effectively. Exceptions may occur in the surface mixed layer, or in areas with a deep winter convection, or in special regions where the density field is more a function of salinity than of temperature.

Redi (1982) suggested that mesoscale mixing could be parametrized in coarse resolution models of the ocean by tilting the lateral mixing so that it is aligned with the isopycnal surfaces. The application of this new parametrization to ocean climate models, that are not detailed enough to represent mesoscale eddies explicitly, has begun and appears to be highly promising.

9. Discussion

Physical oceanography is in a state of transition. Traditionally, ocean circulation studies have been based on the detailed analysis of a rather small number of observations of water mass properties, gathered with meticulous attention to detail over many decades. A remarkable picture of the circulation of the World Ocean has emerged, but it is still essentially qualitative. A new age of ocean measurements, based on ships of opportunity and satellites, promises to greatly expand the data base for ocean circulation studies. There is an urgent need to develop numerical models to be used for data assimilation and interpretation.

The development of ocean models has proceeded slowly, not just because of the limited data base, but also because the ocean has a much greater range of space and time scales to be resolved than has the atmosphere. Kinetic energy is somewhat concentrated at the scale of the radius of deformation in both the atmosphere and the ocean, but the radius of deformation in the ocean is only 1/10 of that in the atmosphere. This implies that a model of the ocean must have ten times the spatial resolution of an atmospheric model to simulate correctly the energy levels of major currents like the Gulf Stream. Not only is the ocean more broad banded than the atmosphere in terms of spatial wave numbers, but it also has significant variability over a broader band in frequency space as well. It is significant that important progress in verifying ocean models against observations has been made in equatorial areas where the time scales are shorter and the spatial scales are longer than in middle latitudes (Richardson and Philander 1987).

As pointed out by Rhines (1986), *PV* is an extremely useful quantity for the verification of circulation models and for physical interpretation. The traditional water mass measurements provide a very useful data set when potential vorticity is mapped

onto density surfaces. Quasi-geostrophic, eddy-resolving models illustrate the very important role of baroclinic instability in the downward transfer of momentum. Because layered quasi-geostrophic models linearize the stratification, they cannot simulate the intersection of isopycnal layers with the ocean surface. Hence, they cannot include the direct downward pathways by which surface *PV* can be injected into the main thermocline of the subtropical gyre. Quasi-geostrophic models are also unable realistically to include the range of processes by which buoyancy sources and sinks change the *PV* field.

The observed patterns of *PV* tend to be uniform at the base of the thermocline in the North Atlantic and Pacific, but in the middle and upper thermocline there are distinctive *PV* patterns. These patterns in the upper thermocline are characterized by high *PV* near the eastern and western boundaries of the subtropical gyre, and a large region of low *PV* in the gyre centre associated with inflowing waters which must have undergone wintertime convection. Cox's (1985) eddy-resolving model based on the primitive equations is general enough to simulate these features. An analysis of the *PV* balance in the model shows that the generation of *PV* takes place in middle latitudes and loss of *PV* takes place when stratified water is carried poleward to subarctic regions of strong heat loss and convection. Some of the convected water is carried poleward to form deep water, but the remainder is turned equatorward by the winds and injected into the main thermocline of the subtropical gyre.

Rhines and Young (1982) were the first to be concerned about the origin of the homogeneous *PV* regions of the lower thermocline. They suggest that a relatively small lateral diffusion of *PV* along the isopycnal surfaces in a region of closed, time-averaged streamlines would inevitably lead to homogenized *PV* through shear dispersion. We have discussed two other possible explanations. One is suggested by the originators of the LPS model. Since the waters injected into the deep thermocline formed by convection have a rather uniform *PV* to begin with, there may be little need to invoke a special process within the thermocline to explain the homogenization. The other mechanism is suggested by the eddy-resolving model of Cox (1985) and the analysis of Böning and Cox (1988). It is based on the fact that stirring by mesoscale eddies penetrates more deeply than the time-averaged advection of *PV*. Thus diffusion could dominate the advection of *PV* at the base of the thermocline, erasing any gradients caused by nonuniform injection. In a recent study Dr Dale Haidvogel (personal communication) has computed the diffusivity by mesoscale eddies in the Holland *et al.* (1984) quasi-geostrophic model and concludes that the mixing is strong, rather than weak as envisioned by the RY model. At present observations are insufficient to allow a clear test which could discriminate between the RY, LPS and Cox mechanisms. The proposed 'gyre-scale experiment', a sub-programme of the large World Ocean Circulation Experiment planned for 1990–1995, is an attempt to resolve this and related issues in gyre dynamics.

The role of the mesoscale eddies in the global heat balance remains uncertain and controversial. Gill (1983) reviewed pertinent data, but was unable to reach any definite conclusion. New computations put this problem in perspective. The mesoscale eddies appear to act primarily as diffusers within, not across, density surfaces. Thus mesoscale eddies in the ocean are very different from synoptic-scale disturbances in the troposphere, which are strongly influenced by non-adiabatic processes, such as radiation and condensation. The solutions suggest that the mesoscale eddies in the ocean are important for transporting heat in the main thermocline only where temperature gradients occur along density surfaces. This situation exists in the polar oceans, but less so in middle latitudes or the tropics.

The importance of any scientific development may be judged by the number of discoveries or developments that it spawns. Ocean modelling is certainly one of the

important offshoots of numerical weather prediction. Numerical modelling is just beginning to have an influence on theories of the ocean circulation and the design of sea-going observational experiments. A deeper understanding of climate requires that ocean and atmosphere models be combined into unified models for the earth's entire fluid envelope.

Acknowledgments

The author wishes to thank Joseph Smagorinsky for encouragement to take on the problem of modelling the ocean circulation. Special thanks also are due to Adrian Gill who was a constant source of new ways of thinking about the ocean. The high scientific standards of Michael Cox have been a constant source of inspiration over the years.

The helpful comments of Isaac Held, Gareth Williams and Peter Rhines, who reviewed an early version of the paper, are deeply appreciated.

References

Bleck, R. and Boudra, D. B. 1981 Initial testing of a numerical ocean circulation model using a hybrid (quasi-isopycnal) vertical coordinate. *J. Phys. Oceanogr.*, **11,** 755–770

Böning, C. and Cox, M. D. 1988 'Particle dispersion and mixing of conservative properties in an eddy-resolving model'. (Available from GFDL)

Brewer, P. G., Broecker W. S., Jenkins, W. J., Rhines, P. B., Rooth, C. G., Swift, J. H., Takahashi, T. and Williams, R. T. 1983 A climatic freshening of the deep North Atlantic (north of 50°N) over the past 20 years. *Science*, **222,** 1237–1239

Bryan, K. 1986 Poleward buoyancy transport in the ocean and mesoscale eddies. *J. Phys. Oceanogr.*, **16,** 927–933

Cox, M. D. 1985 An eddy-resolving numerical model of the ventilated thermocline. *ibid.*, **15,** 1312–1234

Cox, M. D. and Bryan, K. 1984 A numerical model of the ventilated thermocline. *ibid.*, **14,** 674–687

Fuglister, F. C. 1960 Atlantic Ocean atlas of temperature and salinity profiles and data from the International Geophysical Year 1957–1958. *Woods Hole Oceanogr. Inst. Atlas, Ser.* **1,** 209

Gill, A. E. 1983 'Eddies in relation to climate', pp. 441–445 in *Eddies in Marine Science*. Editor A. R. Robinson. Springer-Verlag

Gill, A. E., Green, J. S. A. and Simmons, A. J. 1974 Energy partition in the large-scale ocean circulation and the production of mid-ocean eddies. *Deep-Sea Res.*, **21,** 499–528

Holland, W. R. and Lin, L. B. 1975 On the generation of mesoscale eddies and their contribution to the oceanic general circulation. I: A preliminary experiment. *J. Phys. Oceanogr.*, **5,** 642–657

Holland, W. R., Keffer, T. and Rhines, P. B. 1984 Dynamics of the oceanic general circulation: The potential vorticity field. *Nature*, **308,** 698–705

Hoskins, B. J., McIntyre, M. E. and Robertson, A. W. 1985 On the use and significance of isentropic potential vorticity maps. *Q. J. R. Meteorol. Soc.*, **111,** 877–946

Huang, R.-X. 1987 A three-layer model for wind-driven circulation in a subtropical/subpolar basin. Parts I and II. *J. Phys. Oceanogr.*, **17,** 664–697

Keffer, T. 1985 The ventilation of the world's oceans: Maps of the potential vorticity field. *ibid.*, **15,** 509–523

Levitus, S. 1982 'Climatological Atlas of the World Ocean'. NOAA Prof. Paper 13. Washington, D.C.

Luyten, J. R., Pedlosky, J. and Stommel, H. LPS 1983 The ventilated thermocline. *J. Phys. Oceanogr.*, **13,** 292–309

McDougall, T. J. and Church, J. A. 1986 Pitfalls with numerical representation of isopycnal mixing. *ibid.*, **16,** 196–199

McDowell, S., Rhines, P. B. and Keffer, T. 1982 North Atlantic potential vorticity and its relation to the general circulation. *ibid.*, **12,** 1417–1436

Mintz, Y. 1979 'On the simulation of the oceanic general circulation', volume II of *Performance intercomparison and sensitivity studies*, *Global Research Programme*, W.M.O., Geneva

Munk, W. 1950 On the wind-driven ocean circulation. *J. Meteorol.*, **7,** 79–93

Olbers, D. J., Wenzel, M. and Willebrand, J. 1985 The inference of North Atlantic circulation patterns from climatological data. *Rev. Geophys.*, **23,** 313–356

Redi, M. H. 1982 Oceanic isopycnal mixing by coordinate rotation. *J. Phys. Oceanogr.*, **12,** 1154–1158

Reid, J. L. 1965 *Intermediate waters of the Pacific Ocean.* The Johns Hopkins Oceanogr. Ser., No. 2, The Johns Hopkins Press, Baltimore

Rhines, P. B. 1986 Vorticity dynamics of the oceanic general circulation. *Ann. Rev. Fluid Mech.*, **18,** 433–497

Rhines, P. B. and Young, W. RY 1982 A theory of wind-driven ocean circulation. I. Mid-ocean gyres. *J. Mar. Res.*, **40,** (Suppl.), 559–596

Richardson, P. L. and Philander, S. H. G. 1987 The seasonal variations of surface currents in the tropical Atlantic ocean: A comparison of ship drift data with results from a general circulation model. *J. Geophys. Res.*, **92,** 715–724

Roemmich, D. and Wunsch, C. 1985 Two trans-Atlantic sections: meridional circulation and heat flux in the subtropical North Atlantic Ocean. *Deep-Sea Res.*, **32,** 619–664

Schopf, P. S. and Cane, M. A. 1983 On equatorial dynamics, mixed layer physics and sea surface temperature. *J. Phys. Oceanogr.*, **13,** 917–935

Schott, F. and Stommel, H. 1978 Beta spirals and absolute velocities in different oceans. *Deep-Sea Res.*, **25,** 961–1010

Semtner, A, and Mintz, Y. 1977 Numerical simulation of the Gulf Stream and mid-ocean eddies. *J. Phys. Oceanogr.*, **7,** 208–230

Stommel, H. 1948 On the westward intensification of wind-driven ocean currents. *Trans. Am. Geophys. Union*, **29,** 202–206

Sverdrup, H. U. 1947 Wind-driven currents in a baroclinic ocean: with applications to equatorial currents in the eastern Pacific. *Proc. Nat. Acad. Sci.*, **33,** 318–326

Veronis, G. 1975 'The role of models in tracer studies', pp. 133–146 in *Numerical models of ocean circulation.* Nat. Acad. of Science, Washington D.C.

Welander, P. 1959 An advective model of the ocean thermocline. *Tellus*, **11,** 309–318